Published in final edited form as:
J Nucl Med. 2008 July ; 49(7): 1066–1074. doi:10.2967/jnumed.107.049502.

Antibody mass escalation study in patients with castration resistant prostate cancer using ^{111}I-J591: Lesion detectability and dosimetric projections for ^{90}Y radioimmunotherapy

Neeta Pandit-Taskar[1,2], **Joseph A. O'Donoghue**[3], **Michael J Morris**[4,5], **Eze A. Wills**[2,*], **Lawrence H. Schwartz**, **Mithat Gonen**[6], **Howard I. Scher**[4,5], **Steven M. Larson**[1,2], and **Chaitanya R. Divgi**[1,2,*]

[1]Nuclear Medicine Service, Department of Radiology, Memorial Sloan-Kettering Cancer Center, New York, NY

[2]Department of Radiology, Weill Medical College of Cornell University, 1300 York Avenue, New York, NY

[3]Department of Medical Physics, Memorial Sloan-Kettering Cancer Center, New York, NY

[4]Genitourinary Oncology Service, Department of Medicine, Memorial Sloan-Kettering Cancer Center, New York, NY

[5]Department of Medicine, Weill Medical College of Cornell University, 1300 York Avenue, New York, NY

[6]Department of Biostatistics, Memorial Sloan-Kettering Cancer Center, New York, NY

Abstract

Background—J591, a monoclonal antibody that targets the external domain of the prostate specific membrane antigen (PSMA), has potential as an agent for radioimmunotherapy. A pilot trial was carried out in patients with prostate cancer using repetitive administrations of escalating masses of J591. An analysis was carried out to assess (1) lesion detectability by ^{111}InJ591 gamma camera imaging compared to standard imaging methods and (2) the effect of increasing antibody mass on lesion detectability, biodistribution and dosimetry.

Methods—Fourteen patients with metastatic prostate cancer received escalating amounts (10, 25, 50 and 100 mg) of J591 in a series of administrations each separated by 3 weeks. All antibody administrations included a fixed amount of radiolabeled antibody ^{111}In-DOTA-J591 (2mg of J591 labeled with 185MBq (5 mCi) of ^{111}In via the chelating agent DOTA). Three whole body gamma camera scans with at least one SPECT scan together with multiple whole body count-rate measurements and serum activity concentration measurements were obtained in all patients. Images were analyzed for distribution and lesion targeting. Estimates of clearance rates and liver and lesion uptake were made for each treatment cycle. These estimates were used to generate dosimetric projections for radioimmunotherapy with ^{90}Y-labeled J591.

Results—A total of 80 lesions in 14 patients were detected. Both skeletal and soft tissue disease was targeted by the antibody as seen on ^{111}In-J591 scans. Antibody localized to 93.7% of skeletal lesions detected by conventional imaging. Clearance of radioactivity from whole body, serum and

Corresponding Author: Neeta Pandit-Taskar, MD, Nuclear Medicine Service, Department of Radiology, Memorial Sloan-Kettering Cancer Center, 1275 York Avenue, Box 77, New York, NY 10021, Tel: 212-639-3046, Fax: 212-717-3268.
*Current address: Division of Nuclear Medicine & Clinical Molecular Imaging, Department of Radiology, University of Pennsylvania, Philadelphia, PA 19104.

liver was dependent on antibody mass. Normalized average values of the ratio of residence times between lesion and liver for 10, 25, 50 and 100mg of antibody were 1.0, 1.9, 3.2 and 4.0 respectively.

Dosimetric projections for radioimmunotherapy with ^{90}Y-labeled J591 suggested similar absorbed doses to lesions, for treatment at the maximally tolerated activity (MTA), irrespective of antibody mass. However absorbed doses to liver at MTA would be antibody mass-dependent with estimates of 20, 10, 7 and 5 Gy for 10, 25, 50 and 100mg of J591respectively.

Conclusions—The proportion of the amount of antibody increased in lesions and decreased in the liver with increasing mass of administered antibody up to a dose of 50 mg. Proportional hepatic uptake continued to decrease with increasing antibody mass up to 100 mg. The optimal antibody mass for radioimmunotherapy would therefore appear to be greater than or equal to 50mg.

Keywords

J591 antibody; prostate cancer; radioimmunotherapy; dosimetry

INTRODUCTION

Prostate specific membrane antigen (PSMA) is a 100 kDa transmembrane glycoprotein found on prostate epithelial cells. Both benign and malignant prostatic tissues show excess PSMA expression compared to non-prostatic tissues (1). PSMA expression appears to be greatest in primary prostate adenocarcinoma and nodal metastasis (2,3). Radiolabeled anti PSMA antibody (capromab pendetide, ProstaScint®) has been approved by the FDA for evaluation of metastatic prostate cancer by scintigraphic imaging. ProstaScint antibody targets an internal domain of PSMA and has been used in management of prostate cancer to detect metastatic disease and recurrence (4,5). J591 (Millennium Pharmaceuticals, Cambridge, MA) is a monoclonal IgG1 antibody which targets the external domain of PSMA (6,7) that was derived from the original murine J591 (muJ591) by replacement of the B and T cell epitopes (8). J591 exhibits immune effector function, mainly by inducing antibody dependent cellular cytotoxicity (ADCC) (9). The antibody can be conjugated to a variety of radiometals using the chelating agent 1,4,7,10-tetraazacyclododecane-N,N', N'',N'''-tetraacetic acid (DOTA) (9,10).

Pilot studies to evaluate safety and biodistribution in patients with prostate cancer and solid tumors with extensive neovasculature showed J591 was safe to administer, localized to bone and soft tissue metastatic sites and exhibited dose-dependent hepatic uptake (11–15).

In a phase I study evaluating ^{111}In-J591 in patients with prostate cancer, dose-dependent clearance for administered masses lower than 50 mg was seen, however clearance rates did not differ following repeat administrations over a 4-week period (16).

The feasibility of radioimmunotherapy using J591 has been explored. A Phase 1 dose-escalation radioimmunotherapy study using ^{177}Lu-J591 (370–2590 MBq/ m^2 or 10–70 mCi/ m^2; 10mg/m^2 antibody) showed biodistribution and clearance kinetics similar to ^{111}In labeled J591 antibody (14). Bone marrow was the dose limiting organ with liver as the probable second critical organ for toxicity (14,15). The radiation dose to bone marrow was estimated as 1.2 ± 0.4 cGy/mCi while that to liver was estimated as 7.8 ± 2.2 cGy/mCi (15).

We have previously reported decreasing liver uptake with increasing antibody mass (16,17). In this report, we present an analysis of lesion detection and targeting of ^{111}In-J591 to hormone-refractory prostate cancer, with particular emphasis on the effect of escalating antibody mass on lesion detection, biodistribution and pharmacokinetics. Unique features of this analysis include the comparative lesion and normal tissue pharmacokinetics and dosimetry and the impact of increasing antibody mass on lesion detection with ^{111}In J591. We also evaluated the

feasibility of using this antibody for targeted radionuclide therapy by making dosimetric projections for ^{90}Y-J591 based on the data measured for ^{111}In-J591.

MATERIAL AND METHODS

Patients

A total of 14 patients with metastatic biopsy proven prostate cancer were studied. All patients had progression of disease as determined by rising PSA, increase in lesions on bone scan or either increase in the number of lesions or more than 25% increase in bi-dimensional lesion measurement on CT scan. A minimum PSA of 4 ng/dl was required and a 25% rise in PSA over two measurements obtained 4 weeks apart or three measurements performed one week apart was considered significant for progression. All had received prior therapy with hormones. All patients signed written informed consent. The protocol was approved by the Institutional Review Board of Memorial Sloan-Kettering Cancer Center, the sole study site.

Study Design

This study featured a novel design involving intra-patient mass escalation of administered antibody as described previously (16). Each patient received 4 cycles of J591 with progressively increasing antibody mass . Starting at 10 mg, the mass of administered antibody was increased at three-week intervals; to 25 mg on day 22, 50 mg on day 43, and 100 mg on day 64. All administrations, irrespective of the total antibody mass, included a fixed amount of radiolabeled antibody ^{111}In-DOTA-J591 (2mg of J591 labeled with 185MBq (5 mCi) of ^{111}In via the chelating agent 1,4,7,10-tetraazacyclododecane-N,N',N",N"'-tetraacetic acid DOTA) (16). A total of 14 patients were entered into the study of whom 12 received all 4 infusions of antibody; one patient received 3 antibody infusions (10, 50 and 100mg) and one received 2 antibody infusions (10 and 25mg). All infusions were administered at a rate of ≤ 5 mg antibody/minute (16).

Antibody Radiolabeling

J591 antibody was conjugated with DOTA by direct coupling of one of the four carboxylic acid groups of DOTA to the primary amines present in the protein structure and subsequently labeled with ^{111}In as described previously (10). The specific activity of ^{111}In-DOTA-J591 was approximately 220 MBq/mg (7.6mCi/mg). All radiolabeled material was checked for radiochemical purity using ITLC and immunoreactivity using previously described methods [16]. The radiolabeling yield was more than 85%, radiochemical purity was 99% and immunoreactivity 72% or higher for all administered doses.

Gamma Camera Imaging

Anterior and posterior whole body planar scans were acquired on a Philips dual head gamma camera (Philips Inc., Bothell, WA) using dual energy acquisition centered at 171 and 245 keV with 20% windows. Each patient underwent at least three whole body scans performed on the day of infusion, between day 2–4 and day 5–7 with separate scans of an ^{111}In standard of known activity and background acquired contemporaneously. All patients also had SPECT imaging (64 steps, 40 seconds each) of the chest, abdomen or pelvis to further evaluate sites of uptake from planar imaging or known areas of disease from conventional imaging. SPECT images were constructed using iterative reconstruction and attenuation correction.

Image Interpretation and Lesion Detection

All images were reviewed by Nuclear Medicine physicians, blinded to other conventional imaging results, for tumor targeting. For each patient, anterior and posterior whole body images obtained after each antibody infusion at three time points and SPECT images were visually

analyzed. All visualized areas of uptake were graded on a scale of 1–5 (1=negative, 2=probably negative, 3=equivocal, 4=probably positive, 5 definitely positive). All such areas of uptake were recorded. Baseline CT scans and Tc-99m MDP bone scans were reviewed for lesions by separate radiologists who were blinded to the results of the antibody scans. All lesions detected by each modality were recorded separately. The lesions detected by antibody scans and CT or bone scan were compared.

Whole Body Clearance Measurements

Anterior and posterior whole body count-rates were measured by a 12.7 cm (5 inch) thick sodium iodide NaI(Tl) scintillation detector probe at a fixed geometry (3m from probe to patient). A total of 5–7 measurements were made on each patient from the day of infusion for up to 7 days following antibody administration. The net count rates at later times were normalized to that immediately post-administration (taken as the 100% value) to yield percentage retained activities. These data were used to generate clearance curves and calculate kinetic parameters.

Serum Clearance Measurements

Typically 5 serum samples were obtained: on the day of antibody administration at 5, 15, 30, 60 and 120 min post-antibody infusion, then on at least 3 occasions for up to 7 days following administration. Aliquots of serum were measured in duplicate using a gamma well counter (LKB Wallac, Inc.) together with appropriate ^{111}In standards. Measured activity concentrations were converted to percent injected dose/ liter (% ID/L) and used to generate clearance curves and calculate pharmacokinetic parameters.

Derivation of Whole Body and Serum Kinetic Parameters

Biological and effective clearance rates and corresponding half-times were estimated for each treatment cycle using the SAAM II software application (18). A mono-exponential function was fitted to the whole body data whereas both mono- and bi-exponential functions were fitted to the serum data. Subsequently whole body and serum residence times, τ, were calculated according to the formula $\tau = \tilde{A} / A_0$ where $\tilde{A}$ is the cumulated activity (estimated by integration of the activity-time curve) and A_0 is the administered activity.

Determination of Uptake in Lesions and Liver

Regions of interest (ROI) were drawn on anterior and posterior gamma camera images to encompass the whole body; selected lesions that were clearly seen in both anterior and posterior images and were away from the site of blood pool; whole liver, and normal tissue background. Typically ROI were initially drawn on the latest images acquired after 50 or 100mg antibody infusions (where lesions were generally most clearly seen) then copied and pasted to all other image sets. In all, a total of 24 lesions in 14 patients were examined. Background-corrected geometric mean counts in lesion and liver ROI were computed and expressed as proportions of the geometric mean whole body count. These were converted to proportions of administered activity using the effective whole body clearance curve derived from probe measurement. Residence times in lesions and liver were then estimated by trapezoidal integration. Areas under the terminal portions of the activity-time curves were calculated by extrapolation from the last measured estimate using the apparent terminal clearance rate or physical decay, whichever was the shorter.

In order to assess antibody mass-dependent variations in lesion or liver uptake, a relative uptake parameter was used. Relative uptake was defined as the ratio of residence time in lesion or liver for a particular antibody mass to that for an antibody mass of 10mg. The use of relative

uptakes, calculated for individual patients, minimizes the influence of inter-patient differences and enables more optimal paired statistical comparisons between different antibody masses.

Normal Tissue Dosimetry

Absorbed radiation doses to liver, red marrow and whole body for ^{111}In-DOTA-J591 were estimated using the OLINDA/EXM software application (19). The input data were residence times for liver, red marrow and remainder of body. Residence times for red marrow were derived from serum residence times using standard assumptions (20) namely a proportion of 0.19 of red marrow with a total mass of 1.12 kg, composed of extracellular fluid in equilibrium with serum. On this basis $\tau_{RM} = 0.21\tau_{serum}$ where τ_{serum} is the per-liter value. The residence time for the remainder of body was derived by subtracting liver and red marrow residence times from the whole body residence time. Normal tissue doses were calculated for each patient on a per-cycle basis using individualized kinetics. No adjustments to standard adult male phantom organ masses were made.

In order to assess the potential utility of radioimmunotherapy using ^{90}Y-J591, the projected absorbed doses to normal tissues were estimated, assuming identical biodistribution between ^{111}In- and ^{90}Y-labeled antibodies. Residence times for ^{90}Y-J591 were derived in a similar manner to those for ^{111}In-labeled J591, adjusted for the difference in physical half-lives.

Assessment of Targeting Specificity

For each treatment cycle, the ratios of residence time in lesion to that in liver and the whole body were calculated. The lesion to liver ratio represents targeting specificity with respect to the main antibody sink, whereas the lesion to whole body ratio represents a more generalized assessment of targeting specificity. These ratios were subsequently normalized, for each lesion, to the value for a 10mg antibody dose. Variations in these ratios with antibody mass may be due to changes in uptake and/or retention in lesions, liver and whole body, either individually or in combination.

Projected Absorbed Doses to Lesions for ^{90}Y Radioimmunotherapy

Lesion dimensions were estimated from CT scans for 18 lesions in 12 patients. Lesion volumes were calculated assuming ellipsoidal geometry and lesion mass derived assuming unit density. Subsequently, lesion residence times, corrected for the difference in half-life between ^{90}Y and ^{111}In, were assigned to the CT-derived lesion masses.

Absorbed doses to lesions per unit administered activity (D_l) for ^{90}Y, due only to self-irradiation, were calculated according to the formula $D_l = \Delta\tau_l\phi_l/m_l$, where Δ (= 0.54 g Gy/MBq h) is the absorbed dose per unit cumulated activity concentration for ^{90}Y, τ_l is the ^{90}Y-equivalent lesion residence time, ϕ_l is the lesion size-dependent absorbed fraction for ^{90}Y and m_l is the estimated lesion mass. In order to estimate absorbed fractions, the equivalent lesion spherical radius (for spheres of equal volume to ellipsoids with axes given by the CT lesion measurements) was used to look up ϕ for ^{90}Y from the values tabulated by Bardiès and Chatal (21).

Statistics

Parameter estimates were quoted in terms of mean values and associated standard errors. The statistical significance of differences between groups was assessed using paired t-tests. For lesion detection, detection rates of the three modalities under investigation were compared using McNemar's test. Proportion true positive for each test was evaluated using clinical and radiographic follow-up as the gold standard. Binomial confidence intervals were computed

using the Clopper-Pearson method. Some patients contributed more than one observation and the resulting clustered data were analyzed using methods described by Gonen et al (22).

RESULTS

Fourteen patients with known castration resistant prostate cancer were treated with ^{111}In-J591 (Table 1). ^{111}In J591 antibody scans were positive in all patients for either bone or soft tissue lesions (Figure 1). A total of 90 lesions including 80 bone lesions and 10 soft tissue lesions were detected by either conventional imaging (CT or bone scan) or antibody imaging. Soft tissue lesions involved lymph nodes (n=7) and lung, prostate and seminal vesicle (n=1 each). There were 56 bone lesions detected by CT or bone scan and 8 soft tissue lesions seen by CT scanning. Fifty four (67.5%) osseous lesions were seen on bone scans and 73 (91.25%) on antibody scans (Table 2). CT scan detected 32 skeletal lesions. Six (7.5%) bony lesions seen on bone scans were not seen on antibody imaging and 18 (22.5%) lesions seen on antibody scans were not on bone or CT scan. There was a statistically significant difference for detection of lesions between the imaging modalities (adjusted McNemar's chi square P=0.01). Of the 18 bony lesions identified only on antibody scans, thirteen (16.25%) were confirmed as true lesions on follow up bone scans or CT scans, performed within 4 months after the antibody scan. Eight bony lesions were not seen on antibody scan but were seen on either bone scan or CT scan.

A total of 10 soft tissue lesions were seen on CT scan or antibody scan (Table 2). CT scan detected 8 soft tissue lesions. Antibody study detected 7 lesions. Five lesions were seen on both CT and antibody imaging while CT scan detected 3 lesions not seen on antibody imaging and 2 lesions were seen on antibody imaging only.

Lesions were more evident on antibody scans obtained at later time points after each infusion (Figure 1). Lesions were more detectable on scans obtained with later infusions with higher (50–100mg) antibody masses (Figure 2).

Uptake and Clearance from Whole body, Serum, Liver and Lesions

The clearance of activity from both whole body and serum conformed to monoexponential kinetics with no apparent separate fast and slow clearance phases. Summary statistics are provided in Table 3. For both whole body and serum, biological half-times increased with increasing antibody mass. All inter-group differences with one exception were statistically significant ($P<0.05$) by paired t-test. The sole exception was the difference between whole body biological half-times for antibody masses of 50 and 100mg which fell just outside the significance threshold ($P\sim0.08$),

Residence times for whole body, serum, liver and lesions are also provided in Table 3. For whole body, serum and lesions, residence times increased with increasing antibody mass while for liver they decreased.

As described in Methods, relative uptake parameters (the ratio of residence times normalized to the 10mg level) were used to assess antibody mass-dependent variations in liver and lesion uptake. These are shown in Table 3. For lesions, all inter-group differences were statistically significant except those between antibody masses of 50 and 100mg. For liver, all inter-group differences were statistically significant except those between antibody masses of 25 and 50mg.

Normal Tissue Dosimetry

Estimates of absorbed doses (in mGy/MBq) for whole body, red marrow and liver are provided in Table 4. As described in Methods, the values for ^{90}Y are projections based on the assumption of identical biological behavior between ^{111}In- and ^{90}Y-labeled J591. All inter-group

differences were statistically significant ($P<0.05$) by paired t-test with the following exceptions:

1. For whole body and red marrow, 25 vs. 100mg and 50 vs. 100mg respectively.
2. For liver, 25 vs. 50 mg.

Targeting Specificity

Targeting specificity was assessed using the relative lesion to liver and lesion to whole body residence time ratios. These are shown in Figure 3. The lesion to whole body ratio reached a maximum for an antibody mass of 50mg. In contrast, the lesion to liver ratio continued to increase up to the maximum antibody mass administered (100mg). This latter finding was due to the continual decease in liver residence time rather than an increase in lesion residence time (Table 3).

Dosimetric Projections for ^{90}Y-Labeled J591

Projected absorbed doses (mGy/MBq) to lesions for ^{90}Y-J591 are included in Table 4. The values are for a subset of 15 lesions in 10 patients who received all four administration cycles. The trend here was similar to that observed for lesion residence time and relative uptake with a general increase in lesion absorbed dose from 10–50mg but no further increase from 50–100mg.

We have previously estimated that an absorbed dose to the red marrow of 1.85Gy is close to clinical tolerance for a single administration of ^{131}I-labeled antibody (23). The average administered activities of ^{90}Y-J591 which would result in a red marrow absorbed dose of 1.85Gy were calculated as a function of antibody mass. These are shown in Table 5 together with the corresponding average absorbed doses to liver and lesions. Major differences are apparent between liver absorbed doses for different values of antibody mass with higher doses corresponding to lower antibody masses. In contrast, absorbed doses to lesions appear similar irrespective of antibody mass. This is because the dependencies between antibody mass and red marrow and lesion absorbed doses were similar. It is also apparent (Table 5) that the lesion absorbed dose estimates are very high. This is most likely a consequence of the relatively small lesion mass estimates to which the gamma camera-derived residence times were assigned.

DISCUSSION

7E11, a murine antibody that targets the internal domain of PSMA, is widely utilized to visualize prostate cancer. This antibody (ProstaScint, Cytogen Corporation, Princeton, NJ) is an FDA-imaging agent approved for the detection of occult metastases from prostate cancer. However it is unlikely that 7E11 is taken up by active viable disease due to its binding to the internal domain of PSMA. J591 antibody preferentially binds to the external domain of PSMA and is thus more likely to detect viable prostate tissue.

This report represents an extension and refinement of the initial analysis (16) which reported on toxicity, ADCC induction and clinical antitumor effects in this patient group, together with a preliminary assessment of pharmacokinetics. One of the findings reported previously was that there was no difference in clearance characteristics between mixtures of radiolabeled and “cold” huJ591 antibody when administered either sequentially or concurrently (16). Thus, in the current report, no distinction is made between patients on this basis, and the sole independent variable of interest is the mass of administered antibody. The previous study also reported liver saturation was essentially complete for an antibody mass of 25mg, based on the lack of statistical significance between terminal values of the fraction of whole body counts in the liver for antibody masses ≥25mg. The findings in the current study are more comprehensive

and are based on analysis of full areas under the curve. Based on this analysis, as a proportion of the amount of antibody administered, hepatic uptake continues to decrease up to the highest mass administered i.e., 100mg.

We have quantitatively evaluated the uptake of ^{111}In-J591 in normal tissues and lesions and its dependency on the mass of antibody administered. Various parameters were examined including residence times, relative residence times, lesion to non-lesion residence time ratios and absorbed dose. Irrespective of the parameters used the findings were consistent and may be summarized as follows:

Increasing the mass of antibody administered results in an increased proportion of antibody retained in the circulation, in lesions and in the whole body in general coupled with a reduced proportion retained in the liver.

These results are consistent with the hypothesis that the liver acts as a saturable sink for circulating antibody. Low amounts of antibody are rapidly removed from the circulation leading to relatively low lesion uptake. As the amount of circulating antibody increases the liver gradually saturates, a higher proportion remains in the circulation and the relative lesion uptake increases. In terms of lesion detection, targeting is seen at all dose levels for lesions in both soft tissue and bone. However, in accordance with the quantitative uptake findings, there is increased detection of lesions with increased mass amount of infused antibody. Visually more lesions were detected in delayed scans compared to earlier scans (Figure 1). For any patient, lesions were better detected in the later infusions with higher antibody mass ie the 3rd (50mg) and 4th (100mg) infusions than the first or second infusions (Figure 2). The higher antibody mass scans showed increased number of lesions.

Antibody scans showed good targeting to skeletal disease. As compared to combined CT and bone scan for skeletal lesions, antibody scans detected an additional 13.7% lesions. In comparison to bone scan alone, the results matched in 63% of lesions while 37% of the lesions were discordant ($p=0.01$). In comparison to CT alone, antibody scan detected significantly more lesions ($p=0.01$). There was 45% agreement between antibody and CT scan findings while 37% of lesions were discordant, with more lesions detected on antibody imaging.

Thirteen lesions seen only on antibody scan were confirmed as metastasis on follow-up conventional imaging. Eight lesions seen on bone scan or CT imaging were not seen on antibody scans. Three of these lesions were in pelvic bones overlying sites of blood pool activity in iliac or femoral vessel regions. Four lesions not seen on antibody imaging, represented stable disease as assessed by follow-up scans. Skeletal lesions missed on antibody scans were either small (< 1.5 cm) or in areas with high blood pool background such as the mediastinum or pelvis. Overall, all three modalities differed in detection rates significantly.

The detection rate for soft tissue was low, likely related to small lesion size and location. None of three sites suspected for nodal disease on antibody scan were found to be true lesions on follow up at 6 months. These were located in the neck, pelvis and inguinal region and were likely related to prominent vascular activity. Among parenchymal lesions, antibody scans were able to detect only one lesion located in the peripheral lung. Detection of lung lesions in close vicinity of the cardiac blood pool would generally be limited. Other lesions not detected by antibody imaging were small (< 10 mm) and in the prostate and seminal vesicles.

The potential of J591 as a molecular vector for radioimmunotherapy was assessed by examining the projected absorbed radiation doses for ^{90}Y-labeled antibody based on the quantitative uptake parameters found for ^{111}In-labeled antibody. For a single therapeutic administration the maximally tolerated activity (MTA) of ^{90}Y-J591 will be defined by hematologic toxicity and would thus be expected to be determined by the absorbed dose to red

marrow. On the basis of our analysis it is expected that the MTA of ^{90}Y-J591 would be dependent on the mass of antibody administered. The differences in MTA for different antibody masses may be significant. For example, we estimated the MTA to be around 3300MBq (~90mCi) for 10mg antibody falling to around 2000MBq (~55mCi) for 100mg. Irrespective of the mass of antibody administered, treatment at the MTA would be expected to produce broadly similar absorbed doses to lesions. However there would be major differences in absorbed dose to liver ranging from ~20Gy for 10mg antibody to ~5Gy for 100mg antibody. The possibility of high doses to liver is of particular significance if multiple therapeutic administrations of radiolabeled antibody are contemplated. The hemopoietic system has a significant capacity for regeneration such that similar treatments could be repeated if sufficient time is provided between treatments to allow for recovery. In clinical radiobiologic terms, liver is an example of a “late-responding” normal tissue characterized by long-term “memory” of latent radiation injury and a protracted time-course for the expression of radiation damage. However, liver may also experience significant sparing even for very high average radiation doses, if the dose distribution is spatially non-uniform. It is notable that the use of ^{90}Y with its relatively long-range β-particle emissions would minimize the non-uniformity associated with the dose distribution.

Based on this analysis, a case could be made for defining the optimal mass of antibody to be 100mg, as treatment at the MTA is predicted to result in the lowest absorbed dose to liver while delivering absorbed doses to lesions similar to lower antibody masses. However, it cannot be stated definitively if repetitive treatments at the 100mg level would maintain a high lesion-targeting capability. In the current study, it was found that 100mg of antibody provided high lesion uptake following successive administrations of 10, 25 and 50mg. Thus lesion targeting was maintained for a cumulative antibody mass of 185mg (corresponding to an average of approximately 50mg per administration).

In summary, our data suggest that the optimal mass of J591 antibody for radioimmunotherapy over repeated cycles of treatment is greater than or equal to 50mg and may be as high as 100mg.

CONCLUSIONS

J591 antibody targets both bone and soft tissue lesions. The lesions are best targeted with higher mass amounts of antibody most likely due to the saturation of liver uptake. Similarly, projected data for ^{90}Y-J591 treatment of metastatic lesions in prostate cancer patients suggest that higher antibody masses $\geq$ 50mg would be optimal for radioimmunotherapy. .

Acknowledgments

This study was funded in part by Prostate cancer foundation, the Sacerdote Fund, NCI grant CA10254, and the PepsiCo Foundation for Prostate Cancer.

REFERENCES

1. Murphy GP, Elgamal AA, Su SL, Bostwick DG, Holmes EH. Current evaluation of the tissue localization and diagnostic utility of prostate specific membrane antigen. Cancer 1998;83:2259–2269. [PubMed: 9840525]
2. Sweat SD, Pacelli A, Murphy GP, Bostwick DG. Prostate-specific membrane antigen expression is greatest in prostate adenocarcinoma and lymph node metastases. Urology 1998;52:637–640. [PubMed: 9763084]
3. Silver DA, Pellicer I, Fair WR, Heston WD, Cordon-Cardo C. Prostate-specific membrane antigen expression in normal and malignant human tissues. Clin Cancer Res 1997;3:81–85. [PubMed: 9815541]

4. Rosenthal SA, Haseman MK, Polascik TJ. Utility of capromab pendetide (ProstaScint) imaging in the management of prostate cancer. Tech Urol 2001;7:27–37. [PubMed: 11272670]
5. Petronis JD, Regan F, Lin K. Indium-111 capromab pendetide (ProstaScint) imaging to detect recurrent and metastatic prostate cancer. Clin Nucl Med 1998;23:672–677. [PubMed: 9790041]
6. In vitro characterization of radiolabeled monoclonal antibodies specific for the extracellular domain of prostate-specific membrane antigen. Cancer Res 2000;60:5237–5243. [PubMed: 11016653]
7. Bander NH, Nanus DM, Milowsky MI, Kostakoglu L, Vallabahajosula S, Goldsmith SJ. Targeted systemic therapy of prostate cancer with a monoclonal antibody to prostate-specific membrane antigen. Semin Oncol 2003;30:667–676. [PubMed: 14571414]
8. Hamilton A, King S, Liu H, Moy P, Bander N, Carr F. A novel humanized antibody against prostate specific membrane antigen (PSMA) for in vivo targeting and therapy [abstract]. Proc. Am Assoc. Cancer Res 1998;39:440.
9. Bander NH, Nanus DM, Milowsky MI, Kostakoglu L, Vallabahajosula S, Goldsmith SJ. Targeted systemic therapy of prostate cancer with a monoclonal antibody to prostate-specific membrane antigen. Semin Oncol 2003;30:667–676. [PubMed: 14571414]
10. Smith-Jones PM, Vallabhajosula S, Navarro V, Bastidas D, Goldsmith SJ, Bander NH. Radiolabeled monoclonal antibodies specific to the extracellular domain of prostate-specific membrane antigen: preclinical studies in nude mice bearing LNCaP human prostate tumor. J Nucl Med 2003;44:610–617. [PubMed: 12679407]
11. Bander NH, Trabulsi EJ, Kostakoglu L, Yao D, Vallabhajosula S, Smith-Jones P, Joyce MA, Milowsky M, Nanus DM, Goldsmith SJ. Targeting metastatic prostate cancer with radiolabeled monoclonal antibody J591 to the extracellular domain of prostate specific membrane antigen. J Urol 2003;170:1717–1721. [PubMed: 14532761]
12. Liu H, Moy P, Kim S, Xia Y, Rajasekaran A, Navarro V, Knudsen B, Bander NH. Monoclonal antibodies to the extracellular domain of prostate-specific membrane antigen also react with tumor vascular endothelium. Cancer Res 1997;57:3629–3634. [PubMed: 9288760]
13. Nanus DM, Milowsky MI, Kostakoglu L, Smith-Jones PM, Vallabahajosula S, Goldsmith SJ, Bander NH. Clinical use of monoclonal antibody HuJ591 therapy: targeting prostate specific membrane antigen. J Urol 2003;170(Dec suppl):S84–S89. [PubMed: 14610416]
14. Vallabhajosula S, Kuji I, Hamacher KA, Konishi S, Kostakoglu L, Kothari PA, Milowski MI, Nanus DM, Bander NH, Goldsmith SJ. Pharmacokinetics and biodistribution of 111In- and 177Lu-labeled J591 antibody specific for prostate-specific membrane antigen: Prediction of 90Y-J591 radiation dosimetry based on 111In or 177Lu? J Nucl Med 2005;46:634–641. [PubMed: 15809486]
15. Bander NH, Milowsky MI, Nanus DM, Kostakoglu L, Vallabhajosula S, Goldsmith SJ. Phase I trial of 177lutetium-labeled J591, a monoclonal antibody to prostate-specific membrane antigen, in patients with androgen-independent prostate cancer. J Clin Oncol 2005;23:4591–4601. [PubMed: 15837970]
16. Morris MJ, Divgi CR, Pandit-Taskar N, et al. Pilot trial of unlabeled and indium-111-labeled anti-prostate-specific membrane antigen antibody J591 for castrate metastatic prostate cancer. Clin Cancer Res 2005;11:7454–7461. [PubMed: 16243819]
17. Morris MJ, Pandit-Taskar N, Divgi CR, Bender S, O'Donoghue JA, Nacca A, Smith-Jones P, Schwartz L, Slovin S, Finn R, Larson S, Scher HI. Phase I evaluation of J591 as a vascular targeting agent in progressive solid tumors. Clin Cancer Res 2007;13:2707–2713. [PubMed: 17473203]
18. Barrett PH, Bell BM, Cobelli C, et al. SAAM II: Simulation, Analysis, and Modeling Software for tracer and pharmacokinetic studies. Metabolism 1998;47:484–492. [PubMed: 9550550]
19. Stabin MG, Sparks RB, Crowe E. OLINDA/EXM: the second-generation personal computer software for internal dose assessment in nuclear medicine. J Nucl Med 2005;46:1023–1027. [PubMed: 15937315]
20. Sgouros G. Bone marrow dosimetry for radioimmunotherapy: theoretical considerations. J Nucl Med 1993;34:689–694. [PubMed: 8455089]
21. Bardiès M, Chatal JF. Absorbed doses for internal radiotherapy from 22 beta-emitting radionuclides - beta-dosimetry of small spheres. Phys Med Biol 1994;39:961–981. [PubMed: 15551573]
22. Gonen M, Panageas KS, Larson SM. Statistical issues in analysis of diagnostic imaging experiments with multiple observations per patient. Radiology 2001;221:763–767. [PubMed: 11719674]

23. O'Donoghue JA, Baidoo N, Deland D, Welt S, Divgi CR, Sgouros G. Hematologic toxicity in radioimmunotherapy: Dose-response relationships for I-131 labeled antibody therapy. Cancer Biother Radiopharm 2002;17:435–443. [PubMed: 12396707]

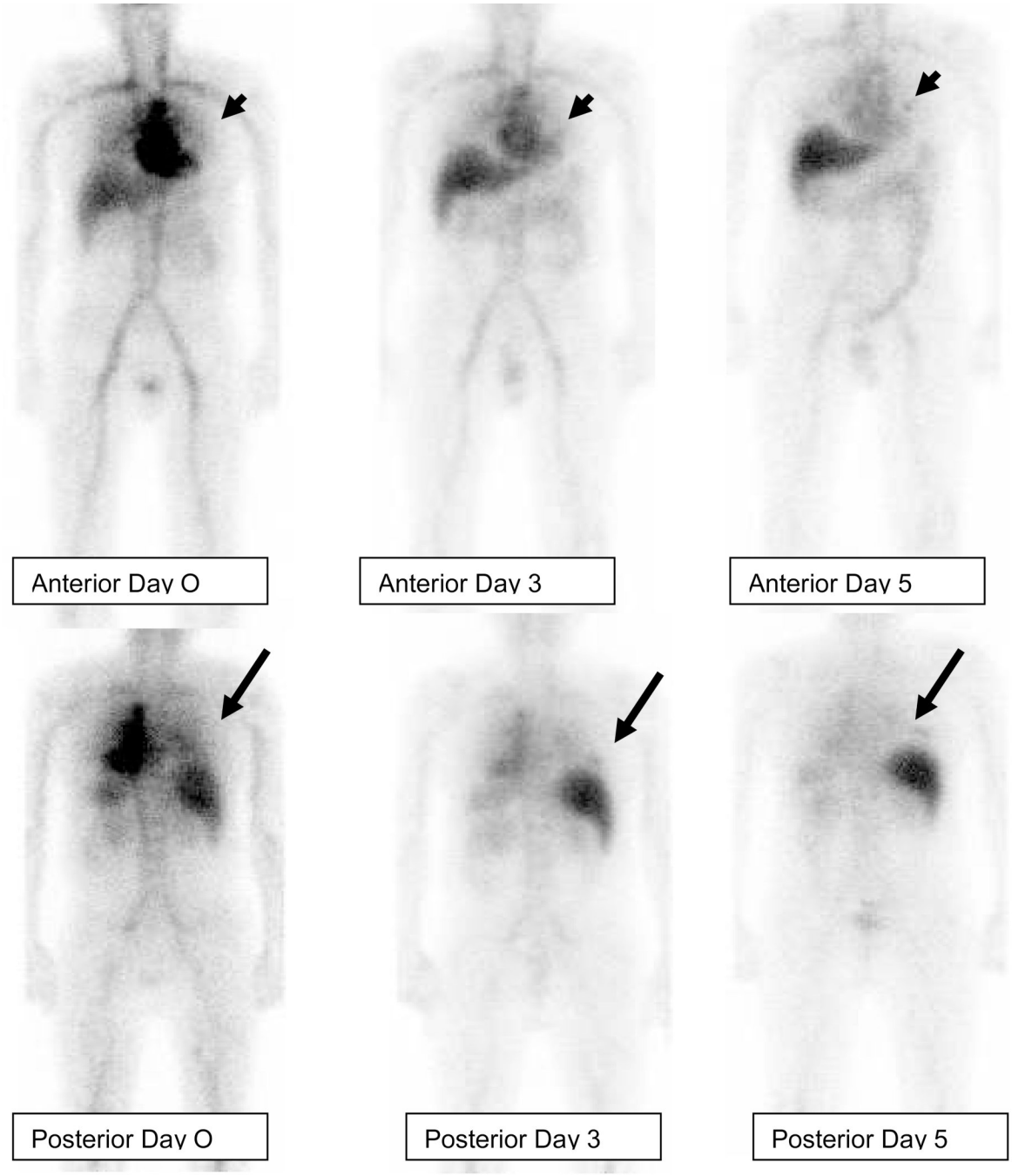

Figure 1.
Patient with metastatic hormone refractory prostate cancer, infused with ^{111}InJ591. Anterior and posterior whole body images were acquired on the day of infusion (day 0), at 72 hrs (day 3) and 120 hrs (day 5) post injection. Uptake of tracer is seen in a left rib lesion (arrow head) anteriorly and right rib lesion posteriorly (arrow). Both these lesions were not seen at all on day 0, faintly visualized on day 3 and clearly visualized on day 5.

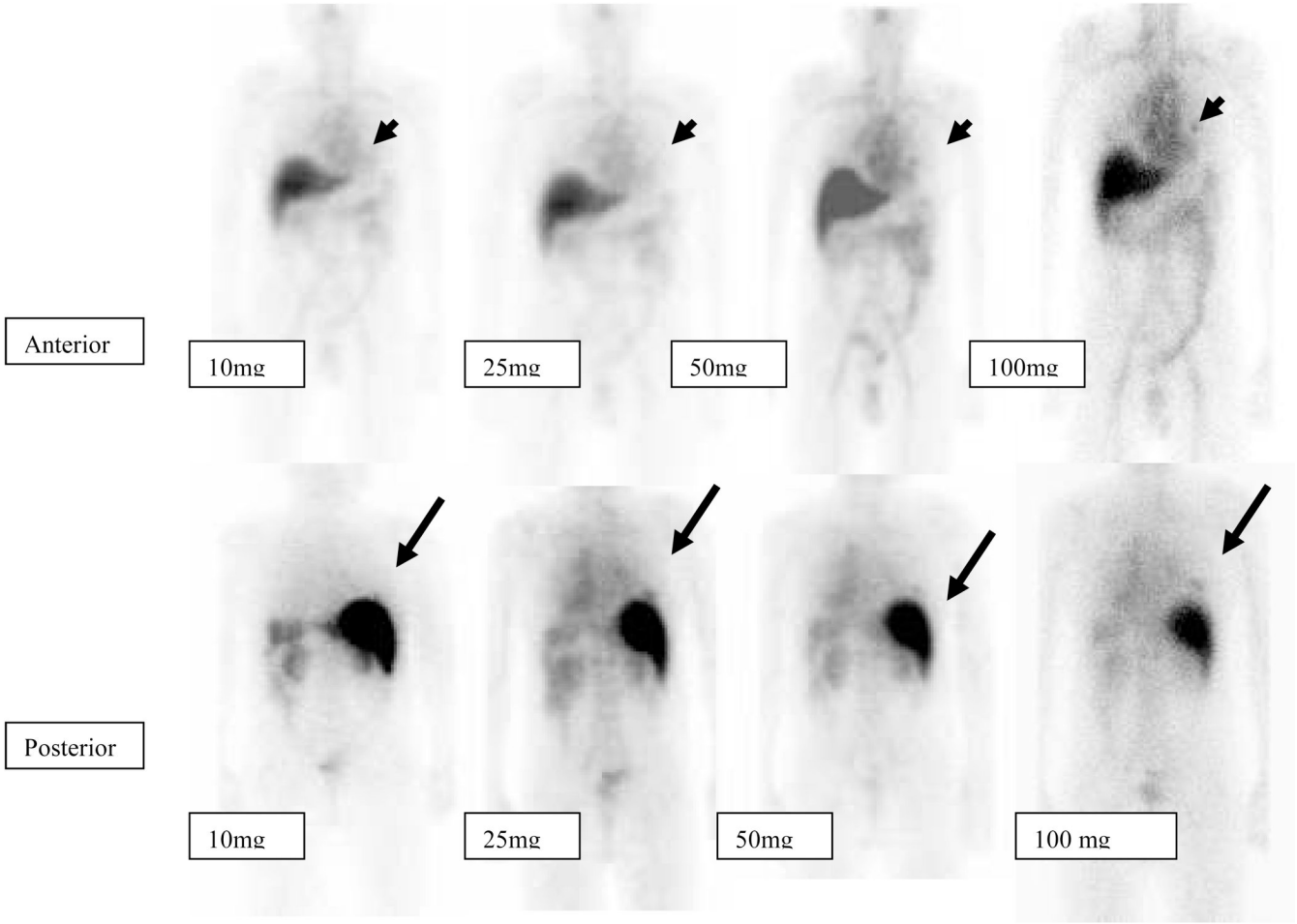

Figure 2.

Patient with metastatic hormone refractory prostate cancer Anterior and posterior whole body images were acquired on the day of infusion (day 0), at 72 hrs (day 3) and 120 hrs (day 5) post injection for each of 10mg, 25mg,50mg and 100 mg of administered antibody. Tracer uptake is seen in a left rib lesion (arrow head) anteriorly and right rib lesion posteriorly (arrow). Both these lesions appear to be more clearly seen in scans with higher antibody infusions (50–100mg) as compared to lesser antibody mass infusions(10,25mg).

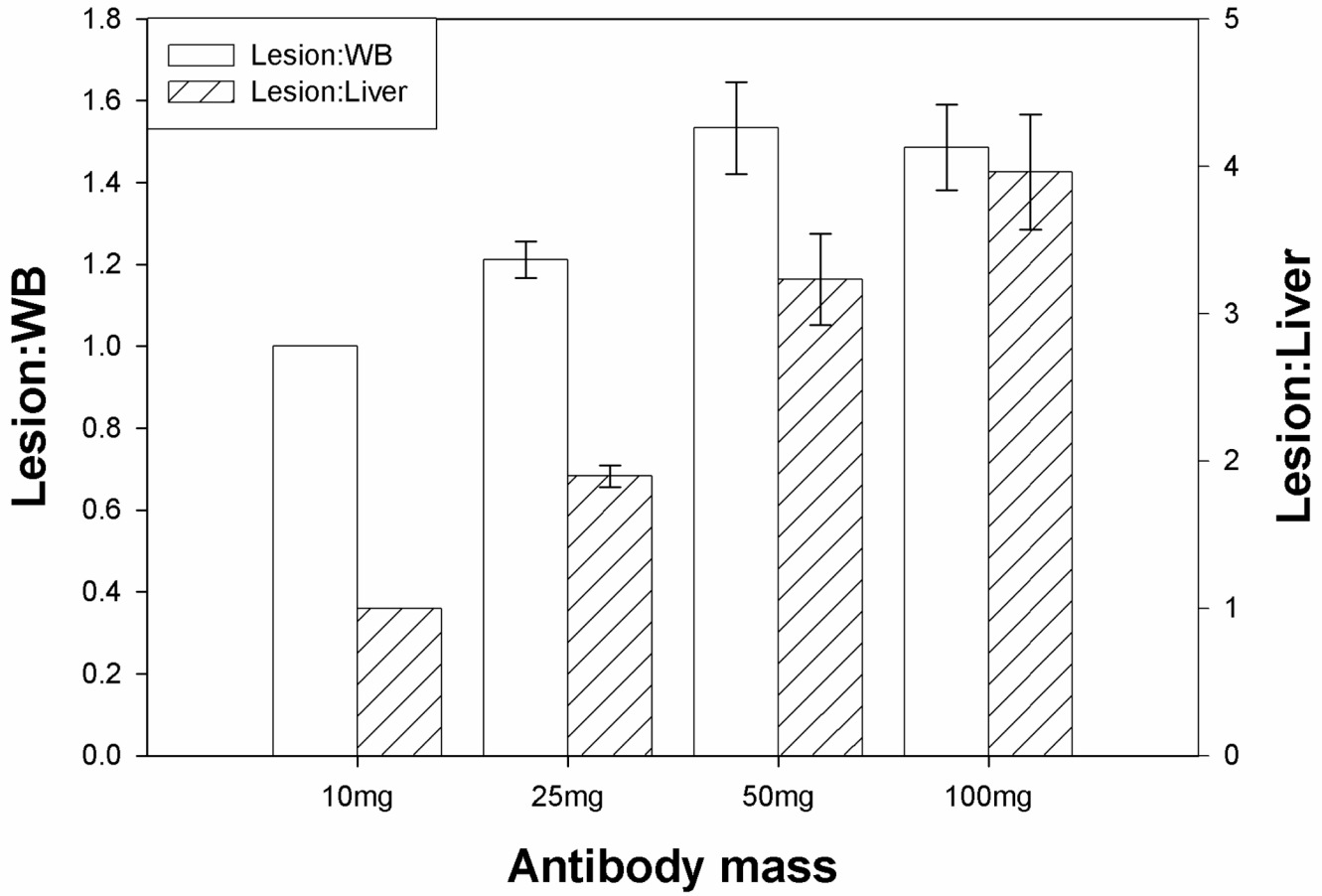

Figure 3.
Relative residence time ratios between lesions and whole body or liver for different administered masses of J591. Error bars are standard errors of the mean. All intergroup differences are statistically significant ($P<0.05$) by paired t-test except lesion:WB for 50mg vs. 100mg.

Table 1

Lesion distribution and detection in patients.

Patients	**No.**
Total	14
Bone metastasis	14
Nodal metastasis	3
Other organ metastasis	2
Scan positive	14
CT scan positive	14
Lesions	
Total lesions: Bone L.Node and organs (soft tissue)	90 80 10
Concordance: bone lesions	
CT or Bone scan positive and antibody scan (Ab) positive	54
CT or bone scan positive, Ab Scan negative	8
CT and bone scan negative, Ab Scan positive	18
Concordance : soft tissue lesions	
CT scan and antibody scan (Ab) positive	5
CT scan positive, Ab Scan negative	3
CT scan negative, Ab Scan positive	2

Table 2

Lesion detection by modality.

Total skeletal lesions (all imaging)	No. of skeletal lesions on bone scan	No. of skeletal lesions on Bone or CT scan	No. of skeletal lesions on Antibody scan	Total soft tissue Lesions on CTscan/Antibody scan	No. of Soft tissue lesions on CT scan only	No. of soft tissue lesions seen on Antibody scan only
7	1	3	7	3	2	3
6	3	3	6	0	0	0
8	5	6	6	0	0	0
8	7	7	7	0	0	0
1	1	1	1	0	0	0
6	3	3	6	0	0	0
3	3	3	2	0	0	0
9	8	9	8	0	0	0
5	3	5	4	0	0	0
7	5	5	7	0	0	0
1	0	1	0	4	4	2
4	2	2	3	3	2	2
6	6	6	6	0	0	0
9	7	7	9	0	0	0
Total						
80	54	61	72	10	8	7

Table 3

Summary of kinetic and uptake data for patients. Values are mean parameter estimates for each administered mass of huJ591. Quoted uncertainties are standard errors of the mean.

	10mg	**25mg**	**50mg**	**100mg**
Whole body $T_{1/2\ biol}$ (days) *	8.5 (± 0.8)	12.8 (± 1.5)	17.7 (± 2.2)	23.1 (± 3.7)
Serum $T_{1/2\ biol}$ (days) §	0.96 (± 0.07)	1.94 (± 0.15)	2.78 (± 0.22)	3.49 (± 0.28)
Whole body residence time (hr)	71 (± 2)	77 (± 2)	82 (± 2)	84 (± 2)
Serum residence time (hr)	24 (± 1)	39 (± 2)	47 (± 2)	53 (± 2)
Liver residence time (hr)	21 (± 1)	15 (± 1)	13 (± 2)	10 (± 1)
Lesion residence time (hr)	0.29 (± 0.05)	0.38 (± 0.07)	0.43 (± 0.06)	0.45 (± 0.08)
Relative liver uptake #	1.0	0.70 (± 0.03)	0.65 (± 0.11)	0.48 (± 0.07)
Relative lesion uptake $	1.0	1.32 (± 0.04)	1.80 (± 0.14)	1.67 (± 0.13)

Statistical significance of the differences between groups assessed by paired t-test:

* all intergroup differences significant ($P<0.05$) except 50mg vs. 100mg

§ all intergroup differences significant ($P<0.05$)

all intergroup differences significant ($P<0.05$) except 25mg vs. 50mg

$ all intergroup differences significant ($P<0.05$) except 50mg vs. 100mg

Table 4

Summary of absorbed dose estimates to whole body, red marrow and liver for ^{111}In-huJ591 and ^{90}Y-huJ591. Values quoted are mean (± standard error of the mean)

Absorbed dose (mGy/MBq)		**10 mg**	**25 mg**	**50 mg**	**100 mg**
Whole body*	^{111}In	0.111 (± 0.003)	0.119 (± 0.003)	0.125 (± 0.002)	0.123 (± 0.006)
	^{90}Y	0.50 (± 0.01)	0.55 (± 0.01)	0.58 (± 0.01)	0.57 (± 0.03)
Red marrow*	^{111}In	0.111 (± 0.004)	0.132 (± 0.005)	0.146 (± 0.004)	0.147 (± 0.008)
	^{90}Y	0.55 (± 0.03)	0.73 (± 0.04)	0.86 (± 0.04)	0.90 (± 0.06)
Liver$	$^{$111}$In	0.75 (± 0.03)	0.56 (± 0.03)	0.48 (± 0.04)	0.37 (± 0.04)
	$^{$90}$Y	5.7 (± 0.3)	4.1 (± 0.3)	3.4 (± 0.4)	2.5 (± 0.3)
Lesion	^{90}Y	58 (± 32)	78 (± 45)	97 (± 53)	95 (± 53)

All intergroup differences were statistically significant (P<0.05) by paired t-test with the following exceptions:

*25 vs. 100mg and 50 vs. 100mg.

$25 vs. 50 mg.

Table 5

Administered activities of ^{90}Y-J591 projected to result in a red marrow absorbed dose of 1.85Gy and corresponding estimates of average absorbed doses to liver and lesions for these administered activities.

	10 mg	**25 mg**	**50 mg**	**100 mg**
Activity of ^{90}Y for red marrow absorbed dose of 1.85Gy (MBq)	3340	2520	2140	2060
Projected absorbed dose to liver (Gy)	19.9	10.3	7.2	5.1
Projected absorbed dose to lesions (Gy)	193	195	208	196